Experimental Methods for Determining Dynamic Stress Intensity Factor in Opaque Materials

A. SHUKLA, H. NIGAM and R. K. AGARWAL
Dynamic Photomechanics Laboratory, Department of Mechanical Engineering, University of Rhode Island, Kingston, RI 02881, USA

ABSTRACT

A review of the various experimental techniques used for determining dynamic stress intensity factors in opaque materials is presented. Dynamic fracture experiments are conducted on heat treated 4340 steel with single edge notch geometry. Instantaneous stress intensity factors as a function of crack length are obtained using the optical techniques of caustics and photoelasticity and also by using strain gages. The results obtained from these techniques are compared.

KEYWORDS

Dynamic stress intensity factor, caustics, photoelasticity, strain gages.

INTRODUCTION

The behavior of a dynamically moving crack is governed by the stress field surrounding it. A moving crack is considered dynamic when the inertial and strain rate effects have significant influence on the stress field. Such is considered the case when the crack speed is of the order of wave speed in the media. For linear-elastic, homogeneous materials it is possible to represent the stress field in the vicinity of a moving crack tip by a single parameter K_{Id}, the dynamic stress intensity factor[1].

There are many methods now available to an experimentalist for evaluating the stress intensity factor for a dynamically moving crack. These methods include both optical and non-optical techniques. Among the optical methods are included, the method of caustics, the method of photoelasticity and the recently developed method of dynamic Moire interferometry. The non-optical methods include the method of using strain gages.

The method of caustics, developed by Manogg[2] is currently used by many researchers[3,4,5]. This technique gives the first term of the series representing the stress field around the crack tip and is related to the stress intensity factor.

The method of transmitted photoelasticity has been used for over 20 years by many investigators[6,7,8]. Over the years many improvements have been incorporated in the analysis technique of photoelastic data to now allow full field evaluation of the stresses around the crack tip[9]. Kobayashi and Dally[10] have demonstrated the successful use of photoelastic coatings on metals. However, the coatings employed by them are useful under diffused light only and the resolution of the photographs obtained is marginal.

Moire interferometry has been recently employed for dynamic applications by Chiang, Deason and Epstein[11,12,13]. Also Kobayashi et al have utilized hybrid experimental numerical techniques for dynamic fracture analysis[14,15].

Electrical resistance strain gage technique suggested originally by Irwin[16] in 1957 for the evaluation of stress intensity factor, is one of the lesser used methods. The primary hesitation in the use of resistance strain gages for fracture studies was their finite size since the crack tip strain field has steep gradients. The averaging effects can be large if the strain gages are not small enough. A detailed study of such averaging effects can be found in[17]. With the availability of extremely small strain gages of sizes less than a millimeter square, it is now possible to accurately measure strains at any point. Recently, Dally and Sanford[18] and Dally and Berger[19] have used strain gages to evaluate stress intensity factor for a stationary crack. In a recent paper Shukla, et al[17] have used strain gages to study dynamic fracture of a brittle polyester material Homalite 100.

In this paper the details of the techniques of photoelasticity, caustics and strain gages as applied to dynamic fracture are discussed. These techniques have then been used to study dynamic fracture of heat treated 4340 steel. The results thus obtained from these experiments are compared.

Experimental Methods and the Analysis Techniques:

The cartesian stress components for a constant speed crack propagating in a finite body can be expressed as[1,20].

$$\sigma_{xx} = \Omega[(1 + 2\alpha_1^2 - \alpha_2^2)\mathrm{Re}Z_1 - \Omega_1\mathrm{Re}Z_2 + (1 + 2\alpha_1^2 - \alpha_2^2)\mathrm{Re}Y_1 - (1 + \alpha_2^2)\mathrm{Re}Y_2] \quad (1)$$

$$\sigma_{yy} = \Omega[-(1 + \alpha_2^2)\mathrm{Re}Z_1 + \Omega_1\mathrm{Re}Z_2 - (1 + \alpha_2^2)\mathrm{Re}Y_1 + (1 + \alpha_2^2)\mathrm{Re}Y_2] \quad (2)$$

$$\tau_{xy} = \Omega[-2\alpha_1\mathrm{Im}Z_1 + 2\alpha_1\mathrm{Im}Z_2 - 2\alpha_1\mathrm{Im}Y_1 + \Omega_2\mathrm{Im}Y_2] \quad (3)$$

where,

$$\Omega = \frac{(1 + \alpha_2^2)}{(4\alpha_1\alpha_2 - (1 + \alpha_2^2)^2)}$$

$$\Omega_1 = \frac{4\alpha_1\alpha_2}{(1 + \alpha_2^2)} \quad (4)$$

$$\Omega_2 = \frac{(1 + \alpha_2^2)^2}{2\alpha_2}$$

$$Z_1 = \sum_{n=0}^{\infty} A_n z_1^{n-1/2} \qquad Z_2 = \sum_{n=0}^{\infty} A_n z_2^{n-1/2} \quad (5)$$

$$Y_1 = \sum_{m=0}^{\infty} B_m z_1^m \qquad Y_2 = \sum_{m=0}^{\infty} B_m z_2^m \quad (6)$$

$$z_1 = x + i\alpha_1 y \qquad z_2 = x + i\alpha_2 y \quad (7)$$

$$\alpha_1^2 = 1 - \left[\frac{\dot{a}}{c_1}\right]^2, \qquad \alpha_1^2 = 1 - \left[\frac{\dot{a}}{c_2}\right]^2 \quad (8)$$

where $\dot{a}$ is the crack velocity, c_1 is the longitudinal wave speed and c_2 is the shear wave speed in the material. The crack tip coordinates, x and y, are oriented such that the negative branch of the x-axis coincides with the crack faces as shown in Fig. 1, and A_n, B_m are unknown real coefficients.

In the various techniques the measurable quantities like the fringe pattern around the crack tip, the diameter of the caustics, the value of strain at a point near the crack tip are related to the stress field parameters (i.e, the series coefficients). Hence from the experimental data the stress intensity factor and other stress field parameters can be obtained.

Method of Photoelasticity

When circularly polarized light passes through a stress birefringent material and then through a circular analyzer, an optical interference pattern of light and dark bands is produced. These bands are referred to as the isochromatic fringes. These fringes are lines of constant maximum in-plane shear stress and are related to the fringe order by the stress optic law, namely

$$2\tau_m = \sigma_1 - \sigma_2 = \frac{Nf\sigma}{h} \quad (9)$$

where σ_1 and σ_2 are in-plane principal stresses, τ_m is the maximum in-plane shear stress, N is the fringe order, f_σ is material fringe value and h is the thickness of the material. For opaque materials a photoelastic coating is applied to the specimen and the same setup of polarizer and quarter wave plate is used as the circular polarizer and the analyzer. The details of the optical setup are shown in Fig.2. The photoelastic coating is made of birefringent material with a reflective backing. Dynamic isochromatic fringes associated with the moving crack are photographed during the experiment. These are then analyzed to obtain the dynamic stress intensity factor.

For analysis the stress optic law is combined with equations (1)-(3) to relate the fringe order and position coordinates at any point in the isochromatic field with the unknown real coefficients A_n and B_m through the expression

$$\left(\frac{Nf\sigma}{2h}\right)^2 = \tau_m^2 = \left(\frac{\sigma_{yy} - \sigma_{xx}}{4}\right)^2 + \tau_{xy}^2 \quad (10)$$

A large number of individual data points from the fringes are used as inputs to an over-deterministic system of non-linear equations of the form of equation (10) and solved in a least-squares sense for the unknown coefficients (A_o,B_o, etc.) by the method suggested by Sanford and Dally[9].

The stress intensity factor is related to the first coefficient by the relation $K_{Id} = A_o\sqrt{2\pi}$. Thus A_o (and consequently K_{Id}) for the stress field in the coating is obtained. A detailed discussion of the analysis procedure is given in Ref.[21]. To obtain the stress intensity factor in the specimen on which the coating is attached it is assumed that the coating strains are equal to the specimen surface strains. With this assumption it can be shown that

$$K_{Id}^{s} = (E^s/E^c)\left(1 + \nu^c\right)/(1+\nu^s)\; K_{Id}^{c} \tag{11}$$

When E is the modulus of elasticity
ν is the Poisson's ratio
Superscripts c and s refer to steel and coating respectively.

Method of Caustics

Unlike the method of photoelasticity, which is based on the interference of light, the method of caustics is based on geometric optics governed by Fermat's principle. When a material with a crack in it is loaded in tension, the high stresses near the crack tip cause the deformation of the body leading to a non-uniform change in the optical path length of the light reflected from its surface. The change in the optical path is due to non-uniform changes in the thickness of the body.

Schematics of the experimental set up used to obtain caustic for opaque materials is shown in Fig.(3). If the light from a point source (the spark) falls on the crack tip region, the image of the crack tip on the reference plane appears as a dark spot surrounded by a bright curve called the caustic curve. The formation of caustic is better seen in Fig.(4).

To determine the stress intensity factor K_{Id} from the experimentally obtained diameter of the caustic, consider an initially planar body lying in the x,y plane at z = 0. Consider light falling normally on the surface z = -f(x,y) of the opaque material as illustrated in figure(4). Let a reference plane (screen) be located behind the reflecting surface at z = -z_o. The mapping of points p(x,y) of the body surface on to points P(X,Y) of the reference plane is given by the following expression[22].

$$\vec{X} = \vec{x} - 2(z_o - f)\left[\frac{\vec{\nabla} f}{1 - (\vec{\nabla} f)^2}\right] \tag{12}$$

which for the case of z_o >>f simplifies to

$$\vec{X} = \vec{x} - 2z_o\,\vec{\nabla} f \tag{13}$$

The deformed shape of the specimen surface reflects the light in such a way that the virtual extension of reflected light rays forms an envelope in space as illustrated in fig(4). The intersection of this envelope with the reference plane is called the caustic curve. The caustic exists if and only if the Jacobian determinant J of the mapping[4] vanishes, i.e.

$$J(x,y,z_o) = det\begin{bmatrix} X_i \\ x_i \end{bmatrix} = 0 \tag{14}$$

The locus points on the specimen surface for which J = 0 is called the initial curve, the points of which map onto the caustic. The out of plane displacement, z = f(x,y), is given by the following relationship:

$$z = -\frac{\nu h}{E}(\sigma_1 + \sigma_2) = -\frac{\nu h}{E}(\sigma_{xx} + \sigma_{yy}) \tag{15}$$

combining equations (1)-(3) with the above equation gives:

$$z = \frac{\nu h}{E} \cdot \frac{K_I^d}{\sqrt{2\pi r_1}} \cdot \cos\frac{\theta_1}{2} \cdot \frac{1}{F(a)} \tag{16}$$

with

$$F(\dot{a}) = \frac{4\alpha_1\alpha_2 - (1 + \alpha_2^2)^2}{(1 + \alpha_2^2)(\alpha_1^2 - \alpha_2^2)} \tag{17}$$

Substituting equation (16) into equations (13) and (14) one can determine the shape of the caustic and can obtain the expression defining the relationship between the stress intensity factor K_{Id}, and the caustic diameter D,

$$K_I^d = \frac{2\sqrt{2\pi}}{3f^{5/2}z_o ch}\; F(\dot{a})\;\; C(\alpha_1)\;\; D^{5/2} \tag{18}$$

where f = 3.17 and c = ν/E and the expression for C is given as:

$$C(\alpha_1) = \frac{(6.8 + 14.4\alpha_1 - 2.6\alpha_1^2)}{18.6} \tag{19}$$

Strain Gage Analysis

The analysis of the strain gage data involves the evaluation of the stress intensity factor from the strain profiles recorded by the gage. The experimental setup used for recording the strain profiles from six strain gages placed along the crack propagation path is shown in figure (5). Using the dynamic stress field representation given by equations (1)-(3), dynamic strain field representation can be derived in a rotated coordinate system by using Hooke's law and appropriate transformation laws[17].

Two coordinate frames are introduced G_{xGyG} and L_{xLyL}, as shown in Fig.(6). The rotated coordinate system G_{xGyG} is fixed to the strain gage and orients itself with it. The coordinate system L_{xLyL} is fixed to the model and is located right below the strain gage on the crack propagation path. In this coordinate frame the crack tip position x_L will be given. The strain gage is considered to be located at an arbitrary point, G(x,y) which is coincident with the strain gage grid center, and rotated at an angle with respect to the coordinate system, O_{xy}. The strain at point G can be determined from the complex strain transformation equation

$$(\epsilon_{yG} - \epsilon_{xG}) + i\gamma_{xGyG} = (\epsilon_{yy} - \epsilon_{xx} + i\gamma_{xy})e^{2i\alpha} \tag{20}$$

and the first strain invariant

$$\epsilon_{xG} + \epsilon_{yG} = \epsilon_x + \epsilon_y \qquad (21)$$

Using Hooke's law along with equations (20), (1,2,3) and eq. (21), we get

$$\epsilon_{xG} = \Omega\frac{(1+\nu)}{E}\left[\frac{(1-\nu)}{(1+\nu)}(\alpha_1^2 - \alpha_2^2)(ReZ_1(z_1) + ReY_1(z_1))\right.$$
$$+ (1+\alpha_1^2)(ReZ_1(z_1) + ReY_1(z_1))\cos(2\alpha)$$
$$- \Omega_1 ReZ_2(z_2)\cos(2\alpha) - (1_1 + \alpha_2^2)ReY_2(z_2))\cos(2\alpha) - (1+\alpha_2^2)ReY_2(z_2))\cos(2\alpha)$$
$$\left. + 2\alpha_1(ImZ_2(z_2) - ImZ_1(z_1) - ImY_1(z_1))\sin(2\alpha) - \Omega\, ImY\,(z\,)\sin(2\alpha)\right] \qquad (22)$$

Setting n = 0 and m = 0 in eq.(5) and eq.(6) and substituting them in eq.(22) yields a two parameter representation of the strain field

$$\epsilon_{xG} = \Omega[A_o[\frac{(1+\nu)}{(1+\nu)}(\alpha_1^2 - \alpha_2^2)\frac{1}{\sqrt{r_1}}\cos(\frac{\phi}{2}) + (1+\alpha_1^2)\frac{1}{\sqrt{r_1}}\cos(\frac{\phi}{2})\cos(2\alpha)$$
$$- \Omega_1\frac{1}{\sqrt{r_2}}\cos(\frac{\phi_2}{2})\cos(2\alpha) + 2\alpha_1\sin(2\alpha)(\frac{1}{\sqrt{r_1}}\sin(\frac{\phi_1}{2}) \qquad (23)$$
$$- \frac{1}{\sqrt{r_2}}\sin(\frac{\phi_2}{2}))] + B_o[(\alpha_1^2 - \alpha_2^2)(\frac{(1-\nu)}{(1+\nu)} + \cos(2\alpha))]\frac{1+\nu}{E}$$

Inspection of eq.(23) suggests that the contribution of B_o term can be set to zero if[17]

$$\cos(2\alpha) = -\frac{(1-\nu)}{1+\nu} \qquad (24)$$

For 4340 steel which has a Poisson's ratio ν, of 0.3 the corresponding α is 118.7°. It is also noted[17] that for these orientations the peak strain occurs when the crack tip is right below the strain gage, i.e., x_L is equal to zero. Now if the strain gage grid lies inside the K_{Id} dominated zone, K_{Id} can be evaluated from the peak strain recorded by a strain gage. A detailed study of the effect of strain gage grid size, orientation etc. can be found in reference[17].

Using peak strain from the dynamic strain profile leads to ($\theta=\phi1=\phi2=90°$ and $\rho1=\rho2=y=h_g$) where h_g is the height of the strain gage above the crack propagation path. Substituting these values in eq.(23) and using the relation $K_{Id} = A_o\sqrt{2\pi}$ yields peak strain, $(\epsilon_{xG})^P$, as a function of K_{Id}

$$(\epsilon_{xG})^P = K_I^d\Omega\frac{(1+\nu)}{2E}\frac{1}{\sqrt{h_g}}\left[\frac{(1-\nu)}{(1+\nu)}(\alpha_1^2 - \alpha_2^2) + \cos(2\alpha)\,((1+\alpha_1^2) - \Omega_1)\right] \qquad (25)$$

Knowing the peak strain from the strain profile, $(\epsilon_{xG})^P$, the crack velocity, a, and measuring the gage orientation, α, and the gage height, h_g, the value of the stress intensity factor, K_{Id} is evaluated.

Experimental Results and Discussion:

Experiments have been conducted with all three techniques discussed above on heat treated 4340 steel specimens. Single edge notch geometry shown in Fig.(7a,b) has been used. The specimen used for photoelastic experiment had face grooves on it. The caustic specimen did not have any faces grooves. Two experiments are performed with strain gages, - with and without face grooves (Fig.7b), to compare the results with the other two techniques.

20 spark gap high speed Cranz-Schardin camera was used to record the caustic and photoelastic patterns. Timings and strain data were recorded on digital oscilloscopes. The specimen material was given the following heat treatment: 20 minutes at 1550°F, oil quenched to 150°F, air cooled to room temperature, and tempered at 650°F for 1 hr. The crack tip was made using a vertical milling cutter. The crack was sharpened using fine angular diamond file.

Photoelastic Experiment

The SEN specimen was loaded to a load of 1.19 kN when the crack initiated. The typical set of pictures from the experiment are shown in Fig(8). The fringe pattern in the coating can be clearly seen. Using the analysis technique discussed before the value of (K_{Id}^s) was estimated. To account for the effect of the groove the following correction suggested by Kobayashi and Dally[10] is used.

$$(K_{Id}^s)^g = K_{Id}^s * F \qquad (26)$$

where $F = \sqrt{(B/B_n)}$

B is the specimen thickness, B_n is the net thickness at the face grooves, g superscript identifies the stress intensity factor associated with the grooved specimen.

The results from this experiment are shown in figure(9). It is seen that K_{Id}^s increases with the crack length as one expects for this geometry. The figure also shows two spikes which are attributed to the stress waves interacting with the running crack tip.

Caustics Experiment

The mirror polished SEN specimen was loaded to 1.71 kN at which load the crack started to propagate. Set of four pictures of the caustics taken from the experiment are shown in fig.(10). The crack velocity was constant at 1063 m/s. The K_{Id} value as a function of crack length to width ratio are plotted in fig.(11). As the crack moves through the specimen the value of the stress intensity factor increases from about 95 MPa$\sqrt{m}$ to 135 MPa$\sqrt{m}$. But when the crack comes too close to the boundary ($\alpha/w<0.85$) the value estimated by this technique drops suddenly.

Strain Gage Experiments

Strain profiles obtained from a typical strain gage experiment are shown in fig(12). The peak strain values are used to evaluate the K_{Id} values. The results for the experiment with face grooves are shown in fig (9) along with the photoelastic results. It is seen that the values of K_{Id} from the

two techniques compare well.

The results from the experiment without the face groove are presented in fig (11) along with the caustics results. Here also it is noticed that the values obtained from the two techniques are close to each other.

Summary

Three of the techniques in current use for the study of dynamic fracture in opaque materials have been presented and discussed. Experimental results obtained with these techniques show that they are in good agreement with each other.

Acknowledgement

The author would like to acknowledge the support of NSF under grant no. MSM-8719567.

References

1. Irwin, G. R., Univ. of Maryland Lecture Notes, 1980.
2. Manogg, P., International Journal of Fracture Mechanics, 2, 1966, pp. 604-613.
3. Theocaris, P. S., Proceedings of IUT Symposium on Optical Methods in Mechanics of Solids, Univ. of Poitires,(1979).
4. Beinert, J. and Kalthoff, J. F.,Mechanics of Fracture, vol. VII, G. C. Sih, ed, Noordhoff Int. Publishing, London, The Netherlands.
5. Rosakis, A. J., Ma, C. C. and Freund, L. B.,Journal of Applied Mechanics, vol. 105, December 1983, pp. 777-782.
6. Dally, J. W.,Experimental Mechanics, vol. 19, No. 10, October 1979. pp. 349-361.
7. Bradley, W. B. and Kobayashi, A. S., Experimental Mechanics, 10(3), 106-113, 1970.
8. Irwin,G.R., et al., Experimental Mechanics, 19, 121-128, 1979.
9. Sanford, R. J. and Dally, J. W., Journal of Engineering Fracture Mechanics, 11, 1979., pp. 621-633.
10. Kobayashi, Takao, and Dally, J. W., Crack Arrest Methodology and Applications,ASTM STP 711,G. T. Han and M. F. Kanninen, Eds., American Society for Testing Materials, 1980,pp.189-210.
11. Chiang, F. P., Dong, B. H. and Lu, H., Proceedings 1985 SEM Spring Conference, pp. 473, 1985.
12. Deason, V., Epstein, J. and Reuter, W. G., Proceedings, 1985 Spring SEM Meeting, pp. 475, 1985.
13. Epstein, J. S., Deason, V. A. and Reuter, W. G.,Proceedings, SEM Fall Conference, "Dynamic Failure", Savannah, GA,pp. 218-217, 1987.
14. Yang, Kwan-Ho and Kobayashi, A. S.,Proceedings of the International Conference on Computational Engineering Science, Atlanta, GA, pp. 48.V.1, 1988.
15. Kobayashi, A. S., Experimental Mechanics, Vol. 23, No. 3, pp. 338-348, Sept. 1983.
16. Irwin, G. R., J. Appl. Mechanics, Vol. 24, No. 3, 1957.
17. Shukla, A, Chona, R., and Agarwal, R. K., Soc. Expt. Mech., Fall Meeting, Houston, 1987.

18. Dally,J.W. and Sanford,R.J., SEM Spring Conference Proceedings 1985, Las Vegas, pp.851-860.
19. Dally, J. W. and Berger, J. R., Proceedings of the 1986 SEM Spring Conference on Experimental Mechanics, New Orleans, June 8-13, 1986, pp. 603-612.
20. Nishioka, T, and Atluri, S. N., Engineering Fracture Mechanics, Vol. 18, No. 1, 1983, pp. 1-22.
21. Shukla, A. and Nigam, H., Engineering Fracture Mechanics, Vol. 25, No. 1, pp. 91-102, 1986.
22. Rosakis, A. J., and Zehnder, A. T., Journal of Elasticity, Vol. 15, 1985, pp. 347-367.

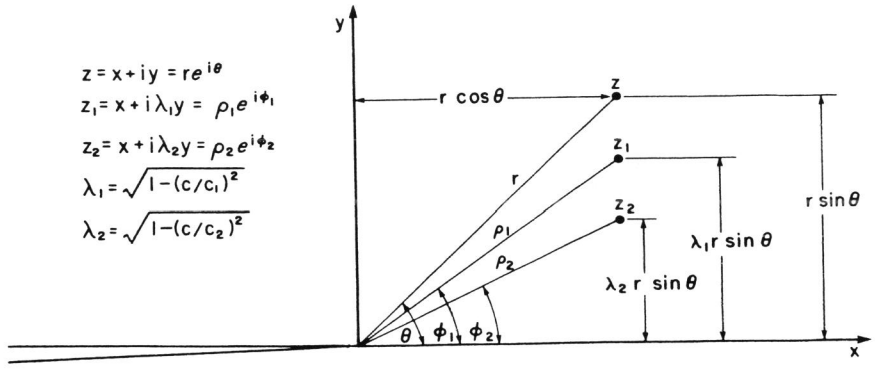

Fig. 1 Coordinate System and Transformation Relations used in the Constant Crack Velocity Analysis

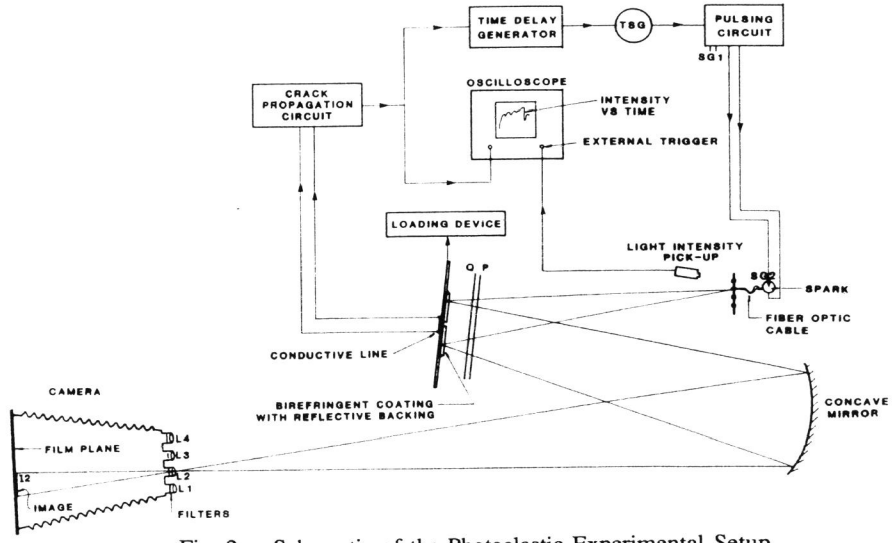

Fig. 2 Schematic of the Photoelastic Experimental Setup

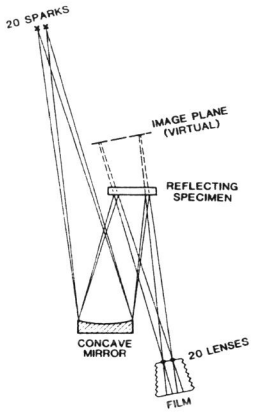

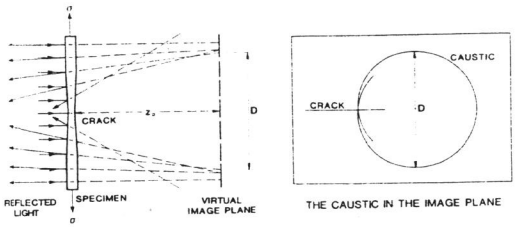

Fig. 4 Formation of a Caustic

Fig. 3 Schematic of the Caustics Experimental Setup

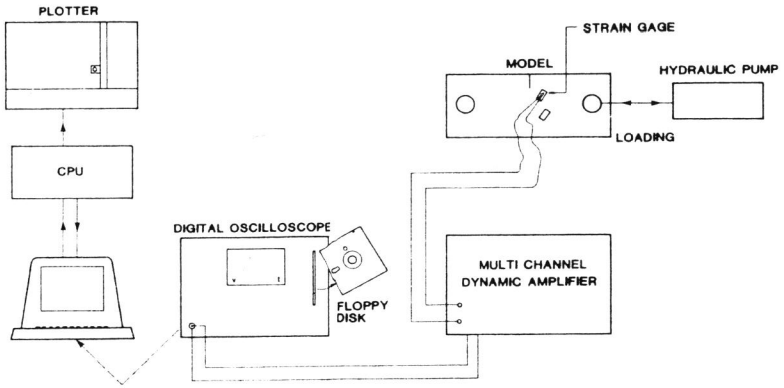

Fig. 5 Schematic of the Strain Gage Experimental Setup

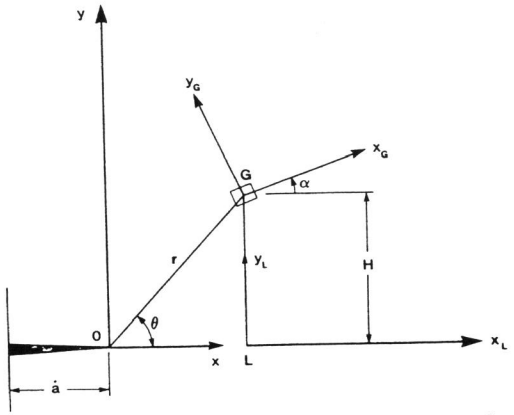

Fig. 6 Coordinate System used for Strain Gage Analysis

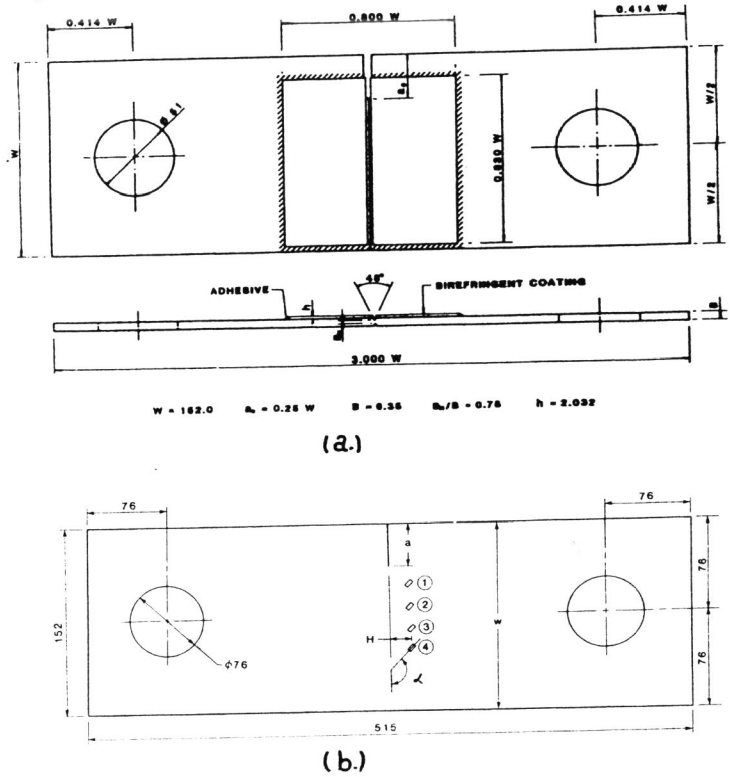

Fig. 7 SEN Specimen Geometries (a) Photoelastic Coating (b) Strain Gages

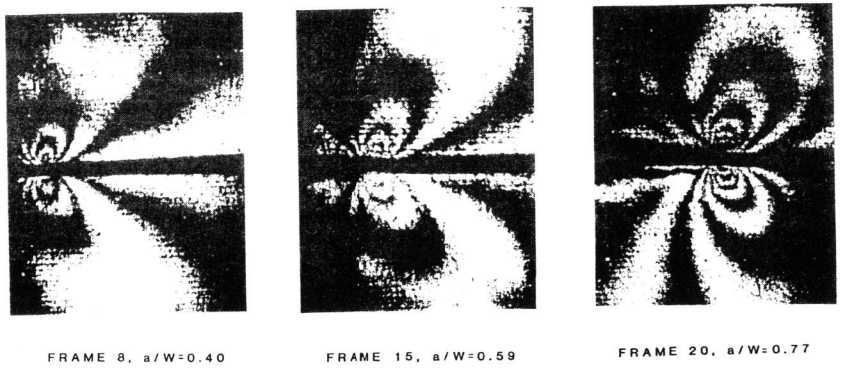

Fig. 8 Typical Isochromatic Fringes Obtained for Steel Specimens

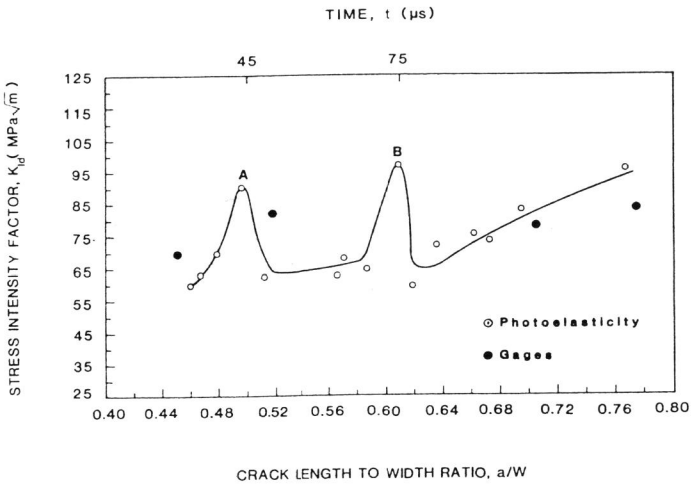

Fig. 9 Stress Intensity Factor as a Function of Crack Length for Photoelastic and Strain Gage Experiments

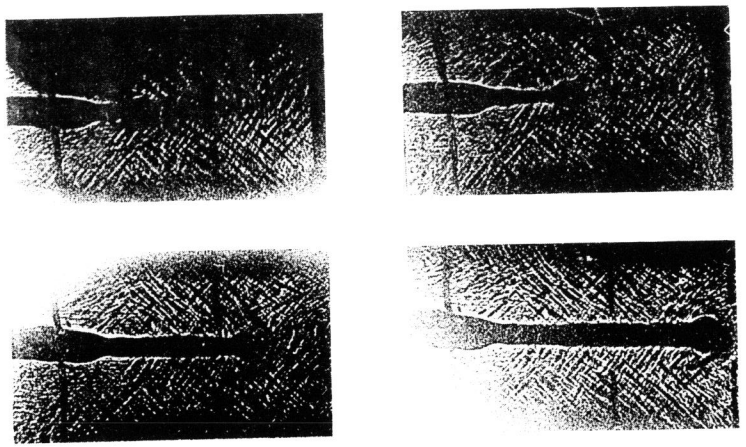

Fig. 10 Typical Caustics Obtained in Steel Specimens

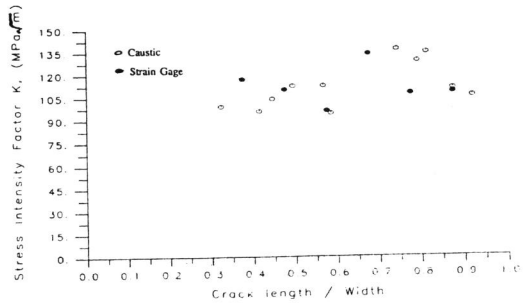

Fig. 11 Stress Intensity Factor as a Function of Crack Length for Caustics and Strain Gage Experiments

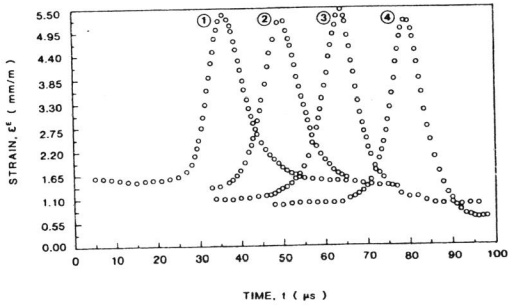

Fig. 12 Typical Strain Profiles Obtained during Dynamic Experiments